IOP Publishing 2D Materials
Journal **XX** (XXXX) XXXXXX https://doi.org/XXXX/XXXX

Graphene setting the stage: Tracking DNA hybridization with nanoscale resolution

Ricardo M. R. Adão[1], Rui Campos[2, ‡] , Edite Figueiras[1, $] , Pedro Alpuim[2,3] and Jana B. Nieder[1,2]

[1] Department of Nanophotonics, Ultrafast Bio- and Nanophotonics Group, INL - International Iberian Nano-technology Laboratory, Av. Mestre José Veiga s/n, 4715-330, Braga, Portugal
[2] Department of Quantum & Energy Materials, 2D Materials and Devices Group, INL - International Iberian Nanotechnology Laboratory, Av. Mestre José Veiga s/n, 4715-330, Braga, Portugal
[3] Department of Physics, University of Minho, Campus de Gualtar, 4710-057, Braga, Portugal
E-mail: jana.nieder@inl.int

Received xxxxxx
Accepted for publication xxxxxx
Published xxxxxx

Abstract

In this study we use nanophotonic effects of graphene to study DNA hybridization: the z^{-4} nanoscale distance-dependence of the fluorescence lifetime for fluorophores located in the vicinity of graphene is for the first time used to track a DNA hybridization reaction with nanoscale resolution in real time. First, a nanostaircase with ~2 nm steps from 0 to a total height of 48 nm is used as a nanoruler to confirm the distance dependence law. We find that the axial sensitivity is suited to determine the nanoscale surface roughness of these samples. The proof-of-concept DNA experiments in aqueous medium involve the hybridization of fluorescently labelled DNA beacons attached to CVD grown graphene with complementary (target) DNA added in solution. We track the conformational changes of the beacons by determining the fluorescence lifetimes of the labelling dye and converting them into nanoscale distances from the graphene. In this way, we are able to monitor the vertical displacement of the label during DNA-beacon unfolding with an axial resolution reaching down to 1 nm. The measured distance increase during the DNA hybridization reaction of about 10 nm matches the length of the target DNA strand. Furthermore, the width of the fluorescence lifetime distributions could be used to estimate the molecular tilt angle of the hybridized ds-DNA configuration. The achieved nanoscale sensitivity opens innovation opportunities in material engineering, genetics, biochemistry and medicine.

Keywords: Biosensor, Graphene, Near-field sensing, Fluorescence quenching, Nanoruler, Fluorescence lifetime spectroscopy

1. Introduction

In the last two decades, several optical microscopy techniques were developed that allowed significant improvement in the lateral resolution of acquired images. In 2014 Hell, Betzig and Moerner were awarded the Nobel Prize in Chemistry for their pioneering work to overcome the optical diffraction limit, creating the field of "Super-resolution microscopy". Prominent techniques include stimulated emission depletion (STED), which reaches down to about 20 nm in lateral resolution, and single molecule localization microscopy (SMLM) techniques, such as photoactivated localization microscopy (PALM), stochastic pptical reconstruction microscopy (STORM) and related techniques, which more recently reached similar resolutions [1]. However, the resolution in the axial (vertical) direction has not been improved accordingly. Typically, the axial resolution only reaches down to 170 nm in STED [2] and with the use of additional optics (typically decreasing the signal detection yield) e.g. via the insertion of a cylindrical lens in SMLM, axial resolutions down to 30 nm were achieved [3].

The ability to achieve high resolution in axial direction on the range of few nanometers, reaching the extension of biological molecules such as proteins or DNA strands is not yet well explored. Such achievement will be of utmost

importance for the study of nanometric features present in biological systems, such as cell membrane topography, organelles, protein complexes and other nanosized biomolecules such as DNA strands. A recent review article summarizes the accomplishments involving axial super-resolution techniques based on near-field interactions between fluorophores and surfaces and highlights their versatility for a variety of future applications [4].

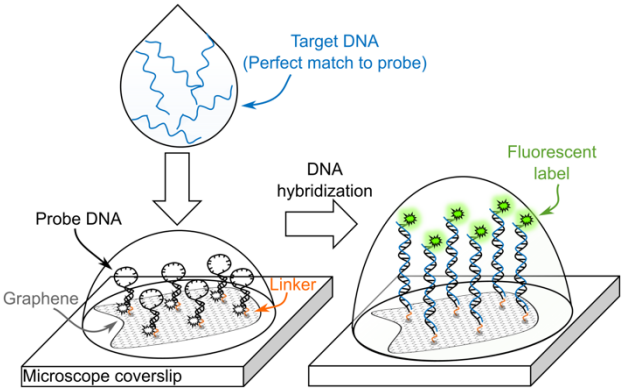

Figure 1. Concept of the proposed Atto488@hp-DNA-Graphene genosensing platform. Initially, before the hybridization with target DNA the beacons are in the folded configuration. Upon the DNA hybridization, the labeling dye is displaced away from the graphene, and its fluorescence is restored in dependence of the nanoscale distance to graphene.

Substrates used to establish near-field distance-dependent contrast so far include metals and more recently, graphene [5]. We propose to use graphene, as a very promising carbon-based biocompatible material for the development of a biosensor with nanoscale resolution.

Biomolecular sensing is crucial for areas like Biomedicine, Food safety, Environmental monitoring and other areas where the detection of traces of biomolecules or DNA can be used for early-stage diagnosis, food quality and authenticity control, or contaminant detection [6]. Biosensing of hybridization chain reactions are key tools in drug development and engineering of complex DNA architectures such and DNA origami [7] with applications in nano-drug delivery, to name just a few examples. Previously reported graphene-based biosensors include electrochemical sensors [8,9], field-effect transistors (FETs) [10–12], as well as fluorescence quenching sensors [13–15]. Most of these sensors rely on the use of graphene oxide colloidal suspensions [16] rather than large-scale graphene sheets, and are characterized by a binary "on-off" operation.

To overcome this limitation and go beyond "on" and "off" state sensitivity we explore for the first time the use of graphene induced near-field effects to distinguish DNA conformations at the nanometer scale, using a functionalized chemical vapor deposition (CVD) - grown graphene surface. The honeycomb lattice of graphene allows the use of linker molecules with aromatic headgroup that stably anchor to the graphene surface via $\pi - \pi$ stacking.

Near-field effects that change the optical properties of emitters in the vicinity of functionalized surfaces have been reported for metallic thin films [17–19], transparent conductive oxides [20] and graphene [5], where the resonant electromagnetic coupling between the electric dipole of an emitter (energy donor) and the occupied electronic states on such surfaces (energy acceptor) enables nanoscale distance-dependent non-radiative resonance energy transfer (RET) from the former to the latter [21,22]. Shorter distances between the acceptor and donor lead to increased RET rates, reduced fluorescence intensity, as well as shortened fluorescence lifetimes.

The nanoscale distance-dependent fluorescence quenching by graphene was first experimentally quantified using nanometer-thin dielectric spacing layers that separated rhodamine dyes from graphene [5]. The obtained relation matches the Chance, Prock and Silbey (CPS) model [23], which formulates the scaling effect of fluorescence lifetime with a z^{-4} dependence at near-field axial distances from graphene [24,25]. So far, the effect has been experimentally tested for selected emitters, including organic dyes [26], quantum dots [27] and semiconductor nanostructures [28], but sensing applications on relevant systems with impact beyond academic interest are lacking. Applications of other near-field effects have been theoretically predicted to produce plasmonic signal enhancement [29] and were applied to a NEMS device [30].

In this work we take the first step in using this effect for the study of biomolecular dynamics. In figure 1 we show the design of the genosensing platform which involves large CVD-grown graphene sheets, functionalized with fluorescently labeled hairpin DNA beacons (hp-DNA). In its initial state, the single-stranded DNA beacon is expected to assume a folded configuration in which the fluorescent labelling dye is placed very close to the graphene – at a distance approximately equal to the length of the linker molecule used to bind the beacon to the graphene.

The DNA hybridization-probing mechanism consists of monitoring at short intervals the fluorescence lifetime of the labeling dye after the addition of the complementary (target) DNA. During the DNA hybridization, the DNA beacons are expected to unfold into a double-stranded extended (vertical) configuration [31], thereby displacing the dye away from the graphene. The measured fluorescence lifetime values are then used to analyze the degree of near field coupling, which scales with the fourth power of the inverse of the distance from the graphene surface (z^{-4} dependence). The distance travelled by the dye should approximately correspond to the molecular length of the DNA strand used. In this work, we perform the proof-of-concept experiments with a 29 nucleotides long DNA strand from a local Port wine grape.

While previous works have demonstrated the graphene-induced nanoscale resolution on nanofabricated static samples we propose for the first time to use the near field quenching effect in the study of the dynamics of a biomolecular system in aqueous environment. This proof-of-concept system is of relevance not only for the study of DNA hybridization kinetics, but indeed for the dynamic observation of conformational change in a vast variety of biomolecules. Such sensing platforms may find applications in various areas of societal relevance - health, security, environment and food authenticity and safety.

2. Experimental Section

2.1 Graphene Fabrication

The graphene used in this work was grown by CVD (EasyTube 3000, FirstNano) on a copper sheet and transferred onto #1.5 microscope glass coverslips. The transfer was performed by removing the graphene from one of the sides of the copper sheet by plasma etching, spin-coating of a poly(methyl methacrylate) (PMMA) support layer on the graphene (16000 RPM; soft-baking temperature 80 °C), dissolution of the Cu in 0.48 M $FeCl_3$ at 35 °C for 30 min, followed by rinsing in 3 cycles of chemical baths (per cycle: 5 minutes in water; 30 minutes in 2% HCl, v/v), manual transfer onto microscope glass coverslip and dissolution of PMMA layer (sample dipped in acetone overnight, followed by a 2 hour 300 °C bake). Further details of the graphene growth and transfer can be found in Ref. [9] by Campos *et al.* Dark field microscopy and Raman confocal microscopy were used to characterize the quality of the sample and results can be found in figure S1 of the Supporting Information (SI).

2.2 Design and Fabrication of a Nanostructured Verification Sample

SiO_2 spacer layers were deposited using Plasma Enhanced-CVD (PE-CVD) (MPX CVD, SPTS) in a stair-like configuration on top of graphene as shown in figure 2(a). Then, 8 successive PE-CVD depositions were performed to create the SiO_2 steps by using a manually-displaced shadow-mask between depositions. Prior to the depositions, the deposition rate of the PECVD was calibrated on auxiliary Si wafer samples using optical reflectometry measurements.

The Atto 488-doped poly vinyl alcohol (PVA) layer was deposited by spin-coating (Spin150, APT), using a 2 µl of 1 mM Atto 488 from Sigma Aldrich in MiliQ water and 400 µl of 0.1% PVA (w/w) in miliQ at 3000 rpm. Ellipsometry measurements (M-2000 Automated Angle (horizontal), Woollam) on an as-prepared sample revealed a film thickness of ~ 2 nm using a two-layer fitting model (SiO_2 Sellmeier native oxide - 3.8 nm; Cauchy thin polymer for the PVA layer: 1.9 nm ± 0.1 nm) in the M-2000 device software. Optical reflectometry measurements were performed using a commercial equipment (NanoCalc XR, Ocean Optics). Atomic force microscopy (AFM) measurements were performed using a commercial equipment (Dimension Icon, Bruker), using tapping mode, resonance frequency of 246.8 kHz, cantilever (PPP-NCH-50, Nanosensors).

Fluorescence lifetime imaging microscopy (FLIM) images were measured on the Atto 488-functionalized step sample. The arrangement of the SiO_2 spacers in steps allows an analysis of the distance-dependent RET process on graphene. FLIM images were taken with 25×25 pixels over areas of 50 µm × 50 µm.

2.3 Graphene bio-functionalization with Atto488@hp-DNA

The binding of hp-DNA molecular beacons to the graphene surface was performed using 1-pyrenebutyric acid N-hydroxysuccinimide ester (PBSE) as linker. The pyrene group of the PBSE binds to graphene non-covalently, but irreversibly and the reactive succinimide ester conjugates with the amino-labeled oligonucleotides of the DNA molecule [32,33]. When the succidimine ester reacts with the amino-labeled oligonucleotides of the DNA molecule, the N-hydroxysuccinimide (NHS) ester group is dropped as a subproduct of the reaction and the 5'-Amino-Modifier C6 binds in its place.

Two buffer solutions were used TSC1: (TSC1) 0.75 M NaCl + 75 mM $Na_3C_6H_5O_7$ (trisodium citrate) and TSC2: 0.30 M NaCl + 30 mM trisodium citrate [34], with pH around 7, as suited for DNA stability [35].

After the transfer of CVD-grown graphene on 18 x 18 mm coverslips, graphene was functionalized with 10 µL of 10 mM PBSE in dimethylformamide (DMF). After 2 hours the surface was rinsed with DMF, H_2O and dried with N_2 stream. Following this, 10 µL of 10 µM probe DNA in TSC1 buffer solution were drop-casted at the same location of the previous drops and left to react overnight *via* NHS reaction with PBSE, at 4 °C. The DNA-modified surface was rinsed with TSC2 buffer solution and passivated with 10 µL of 100 nM of ethanolamine (C_2H_7NO), which were allowed to react for 30 minutes with the PBSE molecules that had not reacted with the amino group of the probe DNA. For the target DNA solution, a concentration of 10 µM in TSC2 was used to ensure that an excess was used when compared to the probe DNA on the surface.

The DNA sequences were, probe: 5' - C6 Amino - AGC TTC ATA ACC GGC GAA AGG CTG AAG CT - Atto 488 - 3' (here: Atto488@hp-DNA), and target: 5' - AGC TTC AGC CTT TCG CCG GTT ATG AAG CT - 3'.

2.4 FLIM Setup and Experimental Parameters

For all FLIM measurements in this study, we use a custom-built FLIM microscope based on time-correlated single photon counting (TCSPC), with a 467 nm picosecond laser (PLP-10, Hamamatsu) at variable repetition rate – typically operated at 20 MHz, coupled to an inverted microscope setup (RM21, MadCityLabs), equipped with an high NA oil immersion objective (CFI plan APO 100x, NA: 1.45, 0.17 WD 0.13, Nikon) with a combined micro- and piezo close loop controlled nanoscanner (NanoLPS200, MadCityLabs), and an avalanche photodiode (APD) (PD50CTD, MPD), which is placed in quasi-confocal configuration with an active surface of 50 µm in diameter.

The TCSPC is implemented using a single-photon counting card (SPC130, Becker&Hickl) to which the sync signal of the pulsed laser controller and the APD detector output are fed. The laser passes a spatial filter, composed of two lenses and a 100 µm pinhole and a 470.0 nm ± 25 nm clean-up filter (470FS10-25, Thorlabs) to block potential background luminescence of the laser source.

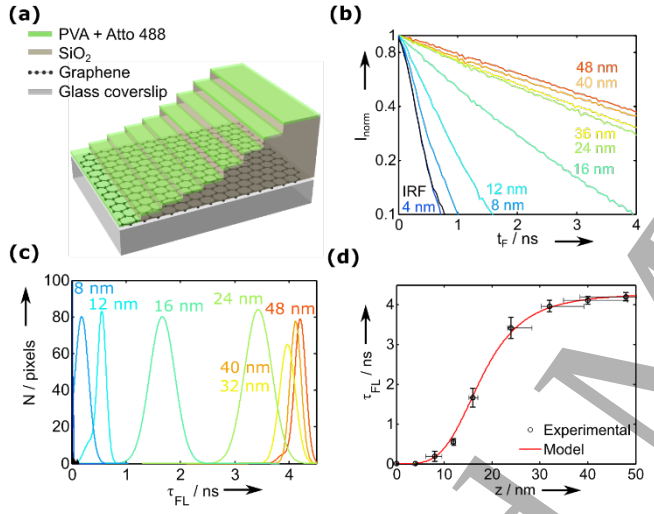

Figure 2. Nano-sensitivity verification. (a) 3D schematic of the verification sample. (b) Integrated Time-Correlated Single Photon Counting (TCSPC) spectra obtained at the discrete SiO_2 steps. (c) Fluorescence lifetime distributions obtained at the discrete SiO_2 steps (set step thickness shown in the labels). (d) Comparison of the mean lifetime values from each distribution (black circles) with a theoretical RET model formulated for graphene by Gaudreau et al. (red curve).[5]

A beam expander is integrated into a cage system at the entry to the inverted microscope. A 480LP Dichroic (F38-482, AHF Analysentechnik) is used to guide the excitation signal to the sample and the fluorescence emission signal towards the detector. Additionally, to block laser excitation from reaching the detector a 472nm long-pass filter (F76-472, AHF) is placed in the detection path before a lens focusing on the detector. A stage top incubator (UNO-T-H-PREMIXED, Okolab) is used to keep the temperature at 21°C and increase the stability of the sample inside the wet chamber.

2.5 FLIM Image Analysis

A "fast fitting of multi-exponential decay curves" algorithm developed by Enderlein at al. [36] was integrated in a custom-made data analysis platform, implemented with a graphical user interface in MATLAB for user-friendly data analysis of FLIM data. The curve-fitting routine deconvolves the experimentally-measured instrument response function (IRF) from the TCSPC spectrum measured at each scanning position, performs a multi-exponential curve fitting and returns an array of exponential coefficients and weighting factors, which we weight-average and color-map to form a FLIM image.

3. Results

3.1 Experimental Verification of Nano-sensitivity

The integrated TCSPC curves obtained from the scans at each spacer layer are plotted in figure 2(b) (the respective FLIM images can be found in figure S3 of the SI). The fluorescence lifetime distribution at each spacer layer (figure 2(c)) was obtained by calculating the histograms of the fluorescence lifetimes determined per FLIM image.

Using Gaussian curve-fittings we calculate the mean and standard deviation of each Gaussian distribution and assign them to the characteristic fluorescence lifetime and associated error of each spacer layer, respectively.

In figure 2(d), the average fluorescence lifetime is plotted as a function of the distance of the Atto488-doped layer to graphene and compared with the z^{-4} distance-dependence RET model developed for graphene by Gaudreau et al. [5] Details regarding the model and the parameters used are presented in Section S3 of the SI. A monotonous distance-dependent reduction of fluorescence lifetime is observed towards shorter distances, which is in excellent agreement with the model (as can be seen in figure 2 (d) and the log-log plot of the same datapoints in figure S4, SI). Iinterestingly, the widths of the fluorescence lifetime distributions shown in figure 2 (c) can be correlated with nanoscale distance distributions which match the surface roughness observed using AFM (see Section S5 of the SI).

Henceforth in this document we use this model (see Equation 7 of the SI) to convert the fluorescence lifetime of the Atto 488 fluorophores into nanoscale distance from the graphene surface.

3.2 "On-Off" Operation of the Genosensing Platform

The mappings of fluorescence intensity (I_F), fluorescence lifetime (τ_{FL}) and nanoscale distance (z) from graphene are shown in figure 3 before (figure 3(a,b,c)) and after (figure 3(d,e,f)) the addition of target DNA, respectively. The distributions of fluorescence intensity are plotted in figure 3(g), the fluorescence lifetime in figure 3(h) and the nanoscale

distance from the graphene surface in figure 3(i). Fluorescence unquenching is visible on the center of the analyzed area, by an intensity increase from 6000 cts/s to 16000 cts/s (figure 3(a,d)), and a lifetime increase from 0.1 ns to about 0.8 ns (figure 3(b,e)). The nanoscale distance distributions in figure 3(i), show for the initial state a Gaussian distribution centered at 1.7 ± 0.3 nm, and for the final state a Gaussian distribution centered at 12.4 ± 0.4 nm.

The displacement of the Atto 488 dyes from the graphene surface, Δz, (figure 3(j)) is calculated by the difference between the nanoscale distance images of the initial and final states. Regions of displacement of the fluorophores where, presumably, the DNA hybridization reaction occurred are clearly distinguishable. We calculate the Δz distribution (figure 3(k)) and use Gaussian curve-fitting to determine the average molecular distance change.

The obtained distribution is dominated by a contribution at Δz around 10.6 ± 0.5 nm and a minor contribution around 8 ± 2 nm. The latter stems from the rims of the emergent feature, as a result of an averaging edge effect due to the finite lateral resolution of the measurements, and can thus be disregarded.

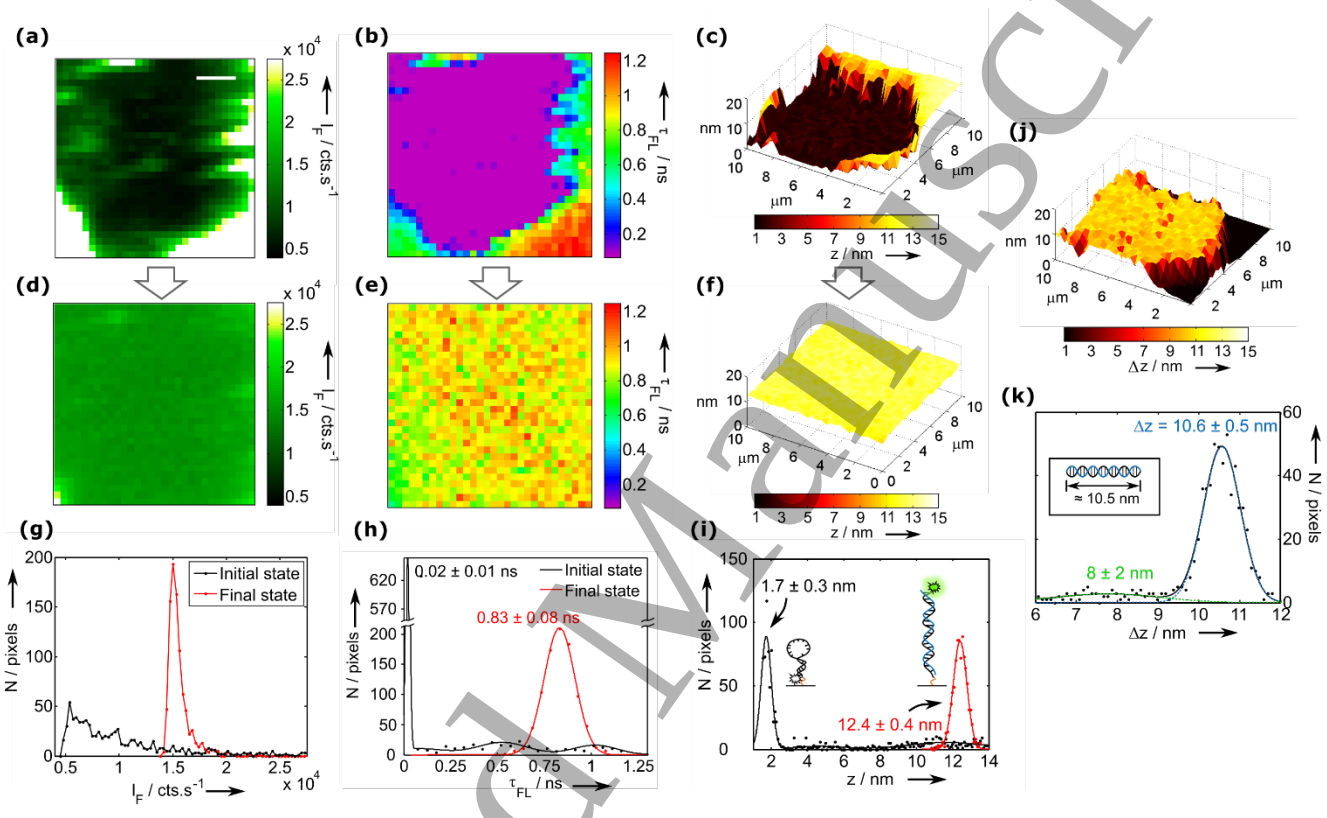

Figure 3. Characterization of the Atto488@hp-DNA-Graphene sensing platform before and ≈ 4 h after addition of target DNA. (a-c) Initial state of the reaction characterized by 2D mappings of the fluorescence intensity: I_F (a), fluorescence lifetime: τ_{FL} (b) and nanoscale distance from the graphene surface: z (c). The latter is calculated from (b) using a theoretical RET model for graphene. [5] The scale bar is 2 μm long, and the same for all images. (d-f) Final state of the reaction characterized by the same quantities and in correspondence with (a-c).The distributions and Gaussian curve-fittings characterizing the initial and final states for each quantity are plotted in (g-i). (j) Nanoscale displacement of the Atto 488 dyes: Δz obtained by subtraction of (f) and (c). (k) Distribution and Gaussian curve-fitting of the Atto 488 displacements

We highlight the substantial agreement firstly between the distribution characteristic of the initial state (1.7 ± 0.3 nm, figure 3(i)) and the estimated 1.7 nm length of PBSE, and secondly between the displacement of the Atto-488 dyes (Δz = 10.6 ± 0.5 nm, figure 3(k)) and the estimated 10.5 nm of molecular length of the DNA strand. The inset graphics of figure 3(i) illustrate DNA beacons in folded and stretched configurations, which can be associated with the initial and final distributions, respectively. Repetitions of the experiments can be found in the SI, Section 7.

3.3 Dynamic Operation of the Genosensing Platform

We perform time-lapse FLIM imaging to dynamically track the molecular displacement of the Atto 488 dyes during DNA hybridization, upon the addition of target DNA to the functionalized graphene surface. In this experiment, 9 measurements were performed, with time intervals of ≈13

minutes (see FLIM images in figure S7, SI). As before, nanoscale distance images and the respective fluorescence lifetimes and nanoscale distance distributions were obtained from the FLIM images [5]. The distributions were fitted using three Gaussian distributions – as can be seen in representative plots associated to three different time points of the series (figure 4(a)). We label the 3 Gaussian distributions as G1, G2 and G3 in correspondence with the initial, intermediate and final distances observed. The resulting curves fitted for of each point of the time-series are plotted in figure 4(b), firstly as line plots (top panel), secondly in color coded 2D representation in dependence of the reaction time t_r (center panel), and thirdly as 2D representation of the three Gaussian distributions (G1, G2 and G3 color coded in blue, green and red, respectively) used in the fittings (bottom panel).

In the initial state, before the addition of target DNA, a single narrow peak is observed, t_r = 0 min (figure 3(i)). However, in the first measurement after the addition of target DNA at t_r = 3 min (figure 4(a)) two distributions can be distinguished, one of them originating in the narrow peak observed at the "off" state (1.9 ± 0.2 nm) and a second broadened distribution around 5 ± 2 nm. Over time, the sharp peak at 1.9 ± 0.2 nm decreases in intensity before vanishing entirely after 92 min, while an initially non-existent peak centered around 10 nm appears and becomes dominant towards the end of the hybridization reaction (total displacement Δz of up to 9 ± 1 nm).

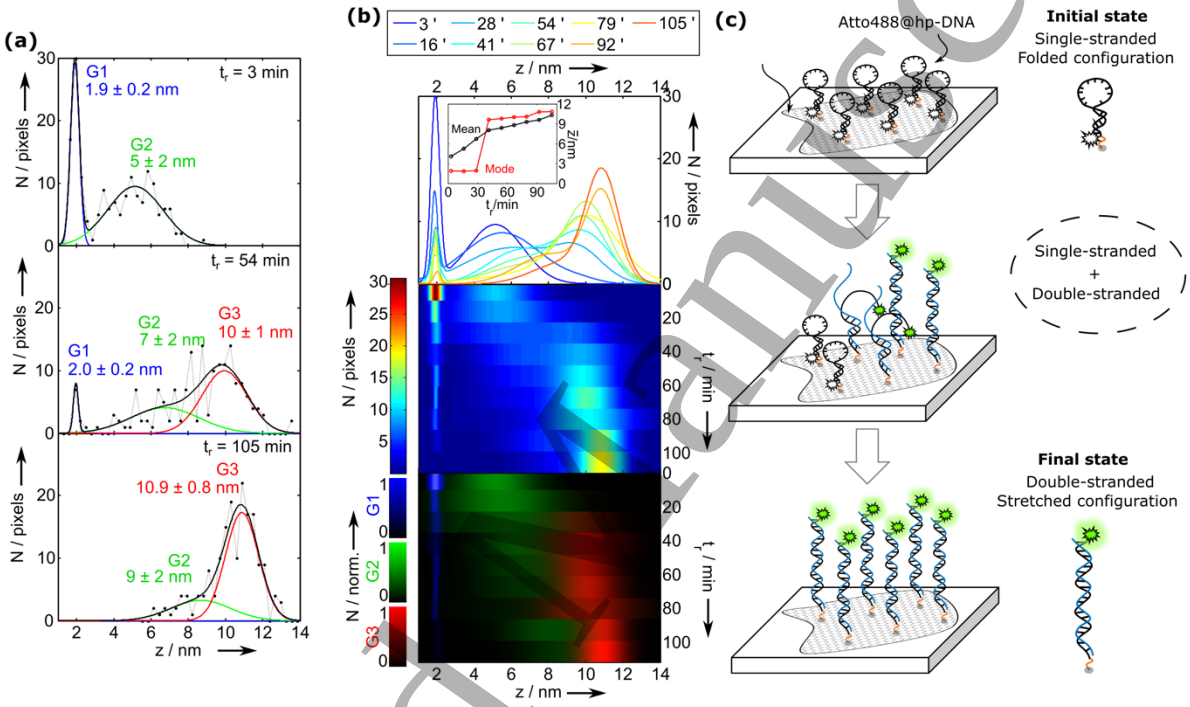

Figure 4. Real-time application of the Atto488@hp-DNA–graphene genosensing platform. (a) Sample of three timestamps of nanoscale distance distributions from time-lapse series taken after addition of complementary DNA, using three Gaussian curve-fittings labeled as G1, G2 and G3. (b) Gaussian fittings for the complete time-lapse series. Top and center panels: the sum of the three Gaussian components; Bottom panel: separate G1, G2 and G3 Gaussian components encoded by a blue, green and red color-code, respectively. Hybridization kinetics is shown in the inset figure, by plotting the mean (black) and mode (red) nanoscale distances over time. (c) Schematic model describing potentially observed dynamic molecular configurations.

Meanwhile, the broadened G2 peak initially observed around 5 ± 2 nm (green contributions in figure 4(b), bottom panel) gradually shifts to a final position at 9 ± 2 nm (t_r = 105 min).

The hybridization kinetics are assessed by plotting the mean and mode of the nanoscale distance distributions over time - inset plot in figure 4 (b), top panel. An abrupt jump in the value of the mode (from 2 to 10 nm) together with a change of slope in the values of the mean as a function of time (from a higher to a lower slope) is observed at reaction time t_r = 40 mins, indicating the conclusion of the hybridization reaction.

In figure 4(c) we summarize our findings in an illustrative way based on the molecular configurations potentially associated to each Gaussian peak used for the dynamic analysis – see Discussion section.

Reproducibility of the ability to observe dynamic changes in time-lapse FLIM images recorded during DNA hybridization reaction, was confirmed (see supplementary time-lapse results in figure S10, SI).

4. Discussion

The results obtained from the nano-staircase verification experiment show an excellent agreement with the theoretical model formulated by Gaudreau et al. [5] We take this as evidence of the sensitivity of the system and suitability of the method to probe near-field interaction changes between the Atto 488 fluorophores attached to DNA molecular beacons and the CVD-grown graphene.

In the static "on-off" experiments (figure 3), the strong variation from very short to longer fluorescence lifetimes upon addition of target DNA, in the central area of the sample, can be associated to initially folded Atto488@hp-DNA that hybridizes and outspreads to an upright extended configuration. During the DNA hybridization, the displacement of the dye away from the graphene is responsible for the partial restoration of the fluorescence lifetime, due to the reduction of the near-field coupling RET efficiency. This interpretation is strongly supported experimentally since the measured displacement of the Atto 488 dyes during DNA hybridization is in agreement with the theoretical predictions. This agreement is verified both for the initial state: 1.7 ± 0.3 nm versus the estimated length of PBSE (≈ 1.7 nm); and for the final state: Δz of about 10.6 ± 0.5 nm versus the estimated length of the selected DNA strand (≈ 10.5 nm).

We highlight the extremely small uncertainty values obtained in the converted nanoscale distance values. While we cannot rigorously guarantee sub-nanometer resolution across the full distance range of this near field sensing method, it is nonetheless remarkable to observe a precision of around 1 nm in the distance range of 1 – 12 nm, as demonstrated by the narrow distance distributions associated with the folded and stretched DNA beacons.

In the analysis of the results, we assume that the stretched DNA configuration is vertically aligned on the graphene plane. However, previous works have shown that 5' bound double-stranded DNA (ds-DNA) may have tilting angles up to 45º [37]. It has also been reported that the vertical alignment of the Atto488@hp-DNA is affected by the density of ds-DNA [8], where higher molecular packing leads to more vertically aligned molecules. In a recent work, we have shown that, under similar conditions, the surface density of this DNA strand on a graphene surface is $1.3\pm0.1 \times 10^{13}$ molecules cm^{-2} (maximum theoretical value of 4.8×10^{14} cm^{-2}) [12], which can be considered high molecular packing conditions, thus restricting the possible angular variance. It has also been reported that the elasticity of the ds-DNA depends on the strand contour length (L) [37,38]. In long DNA strands (L > 50 nm) each base can be seen as a randomly oriented segment, and the elasticity is said to be of entropic nature, and thus affected by temperature. However, short DNA chains (~10.5 nm in our case) can be considered as elastic rods whose bending can be affected by electric potentials, but where temperature effects are negligible [12]. As discussed in Ref. [37] if L << l_p, with l_p being the persistence length that can be determined from $l_p = {\lambda L}/{4}$ ($\lambda = 30$) [38], the duplex behaves like a rigid rod; in our case $l_p \approx 71$ nm and L = 10.5 nm, which confirms the L << l_p condition.

Based on the widths of the initial (FWHM = 0.6 nm) and broader final (FWHM = 0.8 nm) nanoscale distance distributions, we estimate the maximum tilt angle ϕ_{max} for the DNA in the stretched configuration. The estimation relies on the assumption that the axial resolution can be characterized by a Gaussian having the same 0.6 nm width as the narrow distribution. We then fit the broader distribution with the minimum number of such Gaussians. This can be done using three Gaussians separated by FHWM/2 = 0.3 nm, centred at 12.1, 12.4 and 12.7 nm, as can be seen in figure 5 (a). Considering 12.7 nm to be the total molecular length L_T (L_T = DNA length + linker length) in the fully stretched configuration, the shorter 12.1 nm distance could be related to a tilt angle ϕ_{max} by $L_T \cos\phi_{max} = 12.1\ nm$, where $\phi_{max} \approx 18°$, see figure 5 (b). For visualisation purposes, we show in figure 5 (c,d) 3D representations of the modelled semi-spherical surface (L_T = 12.7 nm, ϕ_{max} = 18°) describing the position of the fluorophores on top of rigid rods. The associated numerically calculated z distribution, is plotted in figure 5 (b), black dots.

The obtained total molecular length L_T = 12.7 nm is comparable with our initial estimation of 1.7 +10.5 = 12.2 nm (Section S2 of the SI).

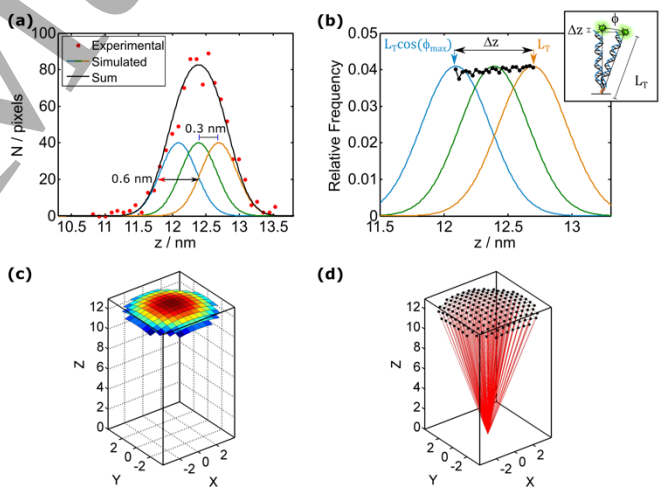

Figure 5. Distribution of angular alignments. (a) Gaussian curve-fitting of nanoscale distance distribution of the final state using 3 sub-resolution Gaussian distributions (FWHM = 0.6 nm, spacing = 0.3 nm). (b) Numerical calculation (black points) of the azimuthal variance ϕ_{max} required to match the range of sub-resolved z-values obtained from the Gaussian curve-fitting in (a). Determined values L_T = 12.7 nm, ϕ_{max} = 18º. (c) Semi-spherical surface used to model the azimuthal variance whose z positions are plotted in (b). (d) 3D representation of the molecular alignment.

In figure 3(c,f) we also observe the presence of dyes located at longer distances above the graphene surface (around 12

nm), that remain nearly unchanged from the initial to the final state of the reaction. This could be related to the presence of defects. Localized defects can form directly during the CVD growth and micro-wrinkles in the graphene sheet may be formed during the transfer process (see enhanced D and G bands in the Raman spectra of defective graphene regions in figure S1, SI) [39,40]. Such defects may lead to a decreased near-field coupling strength between the graphene and the dyes, which weakens the fluorescence lifetime quenching yield of the graphene. As a result, longer, unchanging lifetimes may surge as an artifact of longer distances. Another possibility is the presence of misfolded DNA beacons. Such loop disruptions can be triggered by surface interactions with the functionalized graphene surface [41], or electrostatic forces between neighbor probes [42], particularly in case of high probe densities. As a consequence, these alternate conformations lead to the placement of the dyes at a longer distance from the graphene [43,44], which is not the initial configuration required for this study.

In the dynamic analysis, we assign the sharp and fixed peak (figure 4(a)) at distances of 1.9 ± 0.2 nm to single-stranded (folded) and the broader peak at 10.9 ± 0.8 nm to the double-stranded (stretched) DNA conformations, respectively. We believe that the broad and moving distribution (G2, represented in green in figure 4(a,b)) is the result of the dynamic changes occurring during the hybridization process. As the excitation area of the laser is limited and reaches around 1 μm^2 in the lateral directions, multiple DNA molecules in different hybridization states are probed simultaneously. Therefore the collected signal results from the ensemble emission of the molecules, which might include folded, partly hybridized and fully stretched configurations. The peak shift from an average distance of ≈ 5 nm to ≈ 9 nm over time can be accounted for by the increasing population of molecules approaching the stretched configuration within the excitation area of the laser. Ultimately, the possible heterogeneous conformational states of the ensemble of DNA molecules within the excitation volume cannot be distinguished at the used densities of labeled DNA molecules. However, the observed dynamic range is much larger than the width of the fluorescence lifetime distributions at any time point of the chemical reaction. Also, the converted nanoscale distance distributions are in line with the expected molecular model of an unfolding DNA strand. We thus show that for such synchronized chemical reaction, here triggered by the addition of target DNA, the described fluorescence lifetime method is able to resolve mean molecular conformational changes. To resolve single DNA strand configurations, ultimately a single-molecule sensitive assay is needed. The absence of collective effects at low molecular densities may alter the double-stranded molecular configuration. To overcome such potential differences, alternative assays e.g. using sparsely labeled hp-DNA probes could be devised.

Previous reports have shown that the hybridization kinetics are highly affected by the concentration of the target DNA, temperature and salts concentration in the buffer solution [45]. In our work, despite of the high target concentration, the observed reaction time of approximately 40 minutes is consistent with the rather low temperature of 19° at which the experiments were performed, which significantly decreases the collision frequency of target and probe DNA [46].

To the best of our knowledge, we provide for the first time an axial super-resolution optical image (achieving super-resolution in the vertical direction) of double-stranded DNA on an isolated functionalized graphene flake. We consider this an important sensing achievement with vast applicability in surface bio-functionalization studies and DNA beacon based biosensing. The micrometric lateral resolution enables differentiation between preferential bindings at edges, versus at the flake central region, while the nanometric axial resolution provides topographical information of the DNA strands bound to the graphene.

While previously reported optical super-resolution imaging techniques [47] enable subwavelength lateral resolution, they often provide poor axial resolution – no smaller than around 40 nm [48]. In contrast, we were able to achieve axial resolution down to 1 nm, which can be an outstanding tool for nanometer-scale optical topography measurements. Similar near-field interactions between fluorescent dyes and gold thin films have been used by Chizhik et al. to achieve axial super-resolution in a technique entitled metal-induced energy transfer (MIET)-FLIM. Such technique was used for the study of cell membrane morphology [17] and nuclear membrane architectures [49], with an axial resolution reaching down to 3 - 4 nm, thus demonstrating the great potential in fundamental cell biology and medical sciences. In the present work, the improved axial resolution of about 1 nm via the use of graphene, thereby reaching sub-molecular length scales, provides a new level of sensitivity for biosensing and imaging applications.

Standard topography imaging techniques, such as atomic force microscopy (AFM) have been used to map the distribution of ss-DNA and ds-DNA in functionalized surfaces before and after the hybridization [50], providing information on the conformation of the DNA strands. However, such methods require intrusive probing and are limited to horizontal-lying DNA strands [51,52]. Also, due to the limited penetration capability of the tip, these are rather inadequate for densely packed molecular regimes. Furthermore, such characterization is limited to the comparison between initial and final states of the hybridization reaction, requiring parallel measurements such as X-ray photoelectron spectroscopy (XPS) [50] and fluorescence intensity [51] to assess the status of the hybridization reaction, and thus offering no information regarding the DNA conformation *during* the hybridization. Advantageously compared to such techniques, the approach

described in this work relies on non-intrusive optical probing which allows assessing the heigth of the biological structures, even during hybridization, excluding the need of a reference.

Other advanced DNA biosensing techniques have shown the ability to probe nanoscale information such as determining rotational dynamics of the DNA-bound dye molecule [53]. We take a step further by implementing a method that enables the mapping of the axial position of such dyes, which can be used to probe DNA interactions involving mechanical displacement of the strands, in this case, hairpin-based DNA hybridization. This could be used for the nanoscale imaging of complex biological organizations such as lipid bilayers, using a much simpler apparatus than other super-resolution imaging techniques e.g. scanning near-field optical microscopy (SNOM) [54].

5. Conclusions

We demonstrate that the near field non-radiative coupling between graphene and fluorescent dyes can be used to achieve nanoscale axial resolution in a range of 0 ~ 30 nm using a nanofabricated test sample. The nanoscale sensitivity and analysis of fluorescence lifetime distributions allows the estimation of surface roughness, as demonstrated by comparison with AFM measurements.

Time-dependent measurements allow obtaining real-time DNA hybridization information with axial super-resolution in aqueous solution. The nanoscale distance information enables distinguishing between contributions from folded, stretched and intermediate DNA conformations along the DNA hybridization reaction, which may greatly improve our understanding of the DNA hybridization process.

Our DNA sensing method, employs fluorescence lifetime as the physical quantity, whose value can be used as an absolute measure of the distance of the labelling dye from the graphene. The achieved sensitivity enabled the discussion of possible tilt angles of ds-DNA.

This is a great improvement compared to other DNA sensing platforms which are based on relative measures, e.g. of charge-induced local gating in Field-effect Transistor (FET) based sensing, or fluorescence intensity based sensors that do not carry specific information about molecular reaction states or conformations.

Being a fluorescence-based method, the technology could be converted into an ultrasensitive single-molecule detection method, enabling identification of specific DNA configurations and real-time reaction kinetics at the single DNA strand level. Compared to near field platforms based on thin gold layers of 20 nm thickness and with reported sensitivities of 3-4 nm in axial direction [17], the 2D material graphene is found to reach record breaking of 1 nm axial resolution.

We envision that this nanoscale near field sensitivity of graphene gives the platform the potential to detect misfoldings of DNA strands due to, e.g., mutations in the DNA sequence.

In the limit of high DNA densities the technique will allow the study of complex DNA contact networks. Finally, the fluorescence lifetime susceptibility of fluorescent dyes located in the near field of graphene, a material that exhibits excellent functionalization possibilities [55], may trigger advances in the fields of medicine, food authenticity and safety as well as other biological fingerprinting applications.

Acknowledgements

We are thankful for the fruitful discussions about data analysis procedures with Prof. Dr. Ana Cristina Gomes Silva (FCT-NOVA) and for technical support for Raman measurements from Dr. Fátima Cerqueira (U Minho/INL), for ellipsometry measurements by Dr. Dmitri Petrovykh (INL), for AFM measurments by Dr. Nicoleta Nicoara (INL) and for assistance in the Plasma Enhanced-CVD (PECVD) deposition of SiO_2 layers by Helder Fonseca (INL). Additionally we thank Dr. William Wardley for proofreading and helpful recommendations.

Funding

INL received support for this project from the CCDR-N via the project "Nanotechnology based functional solutions" (grant no. NORTE-01-0145-FEDER-000019) and from the Portuguese Foundation for Science and Technology (FCT) via the project "ON4SupremeSens" POCI-01-0145-FEDER-029417. Edite Figueiras received a Marie Curie fellowship via the EU-EC COFUND program "NanoTRAINforGrowth" (grant no. 600375). U Minho research was partially supported by the FCT in the framework of the Strategic Funding UID/FIS/04650/2013.

Present address

‡ Dr. Rui Campos - AXES Research Group, University of Antwerp, Groenenborgerlaan 171, 2020 Antwerp, Belgium

$ Dr. Edite Figueiras – Fundação Champalimaud, Avenida Brasília, 1400-038 Lisboa - Portugal

References

[1] Huang B, Babcock H eta Zhuang X 2010 Breaking the Diffraction Barrier: Super-Resolution Imaging of Cells *Cell* **143** 1047–58

[2] Willig K I, Harke B, Medda R eta Hell S W 2007 STED microscopy with continuous wave beams **4** 915–8

[3] Juette M F, Gould T J, Lessard M D, Mlodzianoski M J, Nagpure B S, Bennett B T, Hess S T eta Bewersdorf J 2008 Three-dimensional sub – 100 nm resolution fluorescence microscopy of thick samples *Nat. Methods* **5** 527–9

[4] Simoncelli S, Makarova M, Wardley W eta Owen D M 2017 Toward an Axial Nanoscale Ruler for Fluorescence Microscopy *ACS Nano* **11** 11762–7

[5] Gaudreau L, Tielrooij K J, Prawiroatmodjo G E D K, Osmond J, García de Abajo F J eta Koppens F H L 2013 Universal Distance-Scaling of Non-radiative Energy Transfer to Graphene *Nano Lett.* **13** 2030–5

[6] Mehrotra P 2016 Biosensors and their applications - A review *J. Oral Biol. Craniofacial Res.* **6** 153–9

[7] Augspurger E E, Rana M eta Yigit M V 2018 Chemical and Biological Sensing using Hybridization Chain Reaction Chemical and Biological Sensing using Hybridization Chain Reaction

[8] Chalovich J M eta Eisenberg E 2010 Folding-based electrochemical biosensors: the case for responsive nucleic acid architectures *Biophys. Chem.* **43** 496–505

[9] Campos R, Machado G, Cerqueira M F, Borme J eta Alpuim P 2018 Wafer scale fabrication of graphene microelectrode arrays for the detection of DNA hybridization *Microelectron. Eng.* **189** 85–90

[10] Cai B, Wang S, Huang L, Ning Y, Zhang Z eta Zhang G J 2014 Ultrasensitive label-free detection of PNA-DNA hybridization by reduced graphene oxide field-effect transistor biosensor *ACS Nano* **8** 2632–8

[11] Xu S, Zhan J, Man B, Jiang S, Yue W, Gao S, Guo C, Liu H, Li Z, Wang J eta Zhou Y 2017 Real-time reliable determination of binding kinetics of DNA hybridization using a multi-channel graphene biosensor *Nat. Commun.* **8** 14902

[12] Campos R, Borme J, Guerreiro J R, Jr., Machado G, Cerqueira M F, Petrovykh D Y eta Alpuim P 2019 Attomolar Label-Free Detection of DNA Hybridization with Electrolyte-Gated Graphene Field-Effect Transistors *ACS Sensors* **4** 286–93

[13] Ding H, Yu S-B, Wei J-S eta Xiong H-M 2015 Full-Color Light-Emitting Carbon Dots with a Surface-State-Controlled Luminescence Mechanism *ACS Nano* acsnano.5b05406

[14] Lu C H, Yang H H, Zhu C L, Chen X eta Chen G N 2009 A graphene platform for sensing biomolecules *Angew. Chemie - Int. Ed.* **48** 4785–7

[15] Zamora-gálvez A, Morales-narváez E, Romero J eta Merkoçi A 2018 Biosensors and Bioelectronics Photoluminescent lateral fl ow based on non-radiative energy transfer for protein detection in human serum *Biosens. Bioelectron.* **100** 208–13

[16] Morales-narváez E eta Merkoçi A 2019 Graphene Oxide as an Optical Biosensing Platform : A Progress Report *Adv. Mater.* **1805043** 1–12

[17] Chizhik A I, Rother J, Gregor I, Janshoff A eta Enderlein J 2014 Metal-induced energy transfer for live cell nanoscopy *Nat. Photonics* **8** 124–7

[18] Karedla N, Chizhik A I, Gregor I, Chizhik A M, Schulz O eta Enderlein J 2014 Single-molecule metal-induced energy transfer (smMIET): Resolving nanometer distances at the single-molecule level *ChemPhysChem* **15** 705–11

[19] Isbaner S, Karedla N, Kaminska I, Ruhlandt D, Raab M, Bohlen J, Chizhik A, Gregor I, Tinnefeld P, Enderlein J eta Tsukanov R 2018 Axial Colocalization of Single Molecules with Nanometer Accuracy Using Metal-Induced Energy Transfer *Nano Lett.* **18** 2616–22

[20] Moerland R J eta Hoogenboom J P 2016 Subnanometer-accuracy optical distance ruler based on fluorescence quenching by transparent conductors *Optica* **3** 112–7

[21] Förster T 1948 Zwischenmolekulare Energiewanderung und Fluoreszenz *Ann. Phys.* **437** 55–75

[22] Medintz I eta Hildebrandt N 2013 *FRET - Förster Resonance Energy Transfer* (Weinheim: Wiley-VCH, Weinheim)

[23] Chance R R, Prock A eta Silbey R 1978 Molecular Fluorescence and Energy Transfer Near Interfaces *Adv. Chem. Phys.* **37** 1–65

[24] Swathi R S eta Sebastian K L 2008 Resonance energy transfer from a dye molecule to graphene *J. Chem. Phys.* **129** 1–9

[25] Swathi R S eta Sebastian K L 2009 Distance dependence of fluorescence resonance energy transfer *J. Chem. Sci.* **121** 777–87

[26] Gonçalves H, Bernardo C, Moura C, Ferreira R A S, André P S, Stauber T, Belsley M eta Schellenberg P 2016 Long range energy transfer in graphene hybrid structures *J. Phys. D. Appl. Phys.* **49** 315102

[27] Salihoglu O, Kakenov N, Balci O, Balci S eta Kocabas C 2016 Graphene as a Reversible and Spectrally Selective Fluorescence Quencher *Sci. Rep.* **6** 33911

[28] Federspiel F, Froehlicher G, Nasilowski M, Pedetti S, Mahmood A, Doudin B, Park S, Lee J-O, Halley D, Dubertret B, Gilliot P eta Berciaud S 2015 Distance dependence of the energy transfer rate from a single semiconductor nanostructure to graphene *Nano Lett.* **15** 1252–8

[29] Sloan J, Rivera N, Soljačić M eta Kaminer I 2018 Tunable UV-Emitters through Graphene Plasmonics *Nano Lett.* **18** 308–13

[30] Reserbat-Plantey A, Schädler K G, Gaudreau L, Navickaite G, Güttinger J, Chang D, Toninelli C, Bachtold A eta Koppens F H L 2016 Electromechanical control of nitrogen-vacancy defect emission using graphene NEMS *Nat. Commun.* **7** 10218

[31] Li D, Song S eta Fan C 2010 Target-Responsive Structural Switching for Nucleic Acid-Based Sensors *Acc. Chem. Res.* **43** 631–41

[32] Nolan T eta Bustin S A 2016 *PCR technology : current innovations* arg T Nolan eta S A Bustin (CRC Press, Miami)

[33] Kodali V K, Scrimgeour J, Kim S, Hankinson J H, Carroll K M, De Heer W A, Berger C eta Curtis J E 2011 Nonperturbative Chemical Modification of Graphene for Protein Micropatterning *Langmuir* **27** 863–5

[34] Bonanni A, Ambrosi A eta Pumera M 2012 Nucleic acid functionalized graphene for biosensing *Chem. - A Eur. J.* **18** 1668–73

[35] Brown T, Leonard G A, Booth E D eta Kneale G 1990 Influence of pH on the conformation and stability of mismatch base-pairs in DNA *J. Mol. Biol.* **212** 437–40

[36] Enderlein J eta Erdmann R 1997 Fast fitting of multi-exponential decay curves *Opt. Commun.* **134** 371–8

[37] Wang K eta Demaille C 2007 Exploring the Motional Dynamics of End-Grafted DNA Oligonucleotides by in Situ Electrochemical Atomic Force Microscopy 6051–8

[38] Demaille C 2006 Dynamics of Electron Transport by Elastic Bending of Short DNA Duplexes . Experimental Study and Quantitative Modeling of the Cyclic Voltammetric Behavior of 3 ′ -Ferrocenyl DNA End-Grafted on Gold 542–57

[39] Ferrari A C, Meyer J C, Scardaci V, Casiraghi C, Lazzeri M, Mauri F, Piscanec S, Jiang D, Novoselov K S, Roth S eta Geim A K 2006 Raman spectrum of graphene and

graphene layers *Phys. Rev. Lett.* **97** 1–4

[40] Sato K, Saito R, Cong C, Yu T eta Dresselhaus M S 2012 Zone folding effect in Raman G-band intensity of twisted bilayer graphene *Phys. Rev. B - Condens. Matter Mater. Phys.* **86** 1–6

[41] Tan W 2011 Locked nucleic acid based beacons for surface interaction studies and biosensor development **81** 3448–54

[42] Kidambi S, Chan C eta Lee I 2004 Selective Depositions on Polyelectrolyte Multilayers: Self-Assembled Monolayers of m-dPEG Acid as Molecular Template *J. Am. Chem. Soc.* **126** 4697–703

[43] Aalberts D P, Parman J M eta Goddard N L 2003 Single-strand stacking free energy from DNA beacon kinetics *Biophys. J.* **84** 3212–7

[44] Idili A, Ricci F eta Vallée-Bélisle A 2017 Determining the folding and binding free energy of DNA-based nanodevices and nanoswitches using urea titration curves *Nucleic Acids Res.* **45** 7571–80

[45] Zhang J X, Fang J Z, Duan W, Wu L R, Zhang A W, Yordanov B, Petersen R, Phillips A eta Zhang D Y 2018 Predicting DNA Hybridization Kinetics from Sequence *Nat. Chem.* **10** 91–8

[46] Bui H, Shah S, Mokhtar R, Song T, Garg S eta Reif J 2018 Localized DNA Hybridization Chain Reactions on DNA Origami *ACS Nano* **12** 1146–55

[47] Fernández-suárez M eta Ting A Y 2008 Fluorescent probes for super- resolution imaging in living cells **9**

[48] Wöll D eta Flors C 2017 Super-resolution Fluorescence Imaging for Materials Science **1700191** 1–12

[49] Chizhik A M, Ruhlandt D, Pfa J, Karedla N, Chizhik A I, Gregor I, Kehlenbach R H eta Enderlein J 2017 Three-Dimensional Reconstruction of Nuclear Envelope Architecture Using Dual-Color Metal- Induced Energy Transfer Imaging

[50] Casero E, Darder M, Díaz D J, Pariente F, Martín-Gago J A, Abruña H eta Lorenzo E 2003 XPS and AFM characterization of oligonucleotides immobilized on gold substrates *Langmuir* **19** 6230–5

[51] Cattaruzza F, Cricenti A, Flamini A, Girasole M, Longo G, Prosperi T, Andreano G, Cellai L eta Chirivino E 2006 Controlled loading of oligodeoxyribonucleotide monolayers onto unoxidized crystalline silicon; fluorescence-based determination of the surface coverage and of the hybridization efficiency; parallel imaging of the process by Atomic Force Microscopy *Nucleic Acids Res.* **34**

[52] Pastré D, Joshi V, Curmi P A eta Hamon L 2013 Detection of single DNA molecule hybridization on a surface by atomic force microscopy *Small* **9** 3630–8

[53] Backer A, Lee M Y eta Moerner W E 2016 Enhanced DNA imaging using super-resolution microscopy and simultaneous single-molecule orientation measurements **3**

[54] Berweger S, Nguyen D M, Muller E A, Bechtel H A, Perkins T T eta Raschke M B 2013 Nano-chemical infrared imaging of membrane proteins in lipid bilayers *J. Am. Chem. Soc.* **135** 18292–5

[55] Wang Y, Li Z, Wang J, Li J eta Lin Y 2011 Graphene and graphene oxide: Biofunctionalization and applications in biotechnology *Trends Biotechnol.* **29** 205–12